In Situ Labeling of the Aqueous Compartment of Extracellular Vesicles with Luminescent Gold Nanoclusters

Ester Butera, Aurelien Dupont, Alexis Aimé, Solène Ducarre, Regina M Chiechio, Pascale Even-Hernandez, Annalinda Contino, Giuseppe Maccarone, Célia Ravel, Valérie Marchi

ACS APPLIED MATERIALS & INTERFACES

www.acsami.org

Research Article

In Situ Labeling of the Aqueous Compartment of Extracellular Vesicles with Luminescent Gold Nanoclusters

Ester Butera, Aurelien Dupont, Alexis Aimé, Solène Ducarre, Regina M. Chiechio, Pascale Even-Hernandez, Annalinda Contino, Giuseppe Maccarone, Célia Ravel, and Valérie Marchi*

Cite This: *ACS Appl. Mater. Interfaces* 2024, 16, 21643−21652

Read Online

ACCESS | Metrics & More | Article Recommendations | Supporting Information

ABSTRACT: Extracellular vesicles (EVs) are well-known membrane-limited particles secreted by both healthy and cancerous cells. They are considered as biomarkers for early cancer diagnosis and are involved in many pathologies and physiological pathways. They could serve as diagnostic tools in liquid biopsies, as therapeutics in regenerative medicine, or as drug delivery vehicles. Our aim is here to encapsulate luminescent nanoprobes in the aqueous compartment of human EVs extracted from reproductive fluids. The analysis and labeling of the EVs content with easily detectable luminescent nanoparticles could enable a powerful tool for early diagnosis of specific diseases and also for the design of new therapeutics. In this view, gold nanoclusters (AuNCs) appear as an attractive alternative as nontoxic fluorophore probes because of their luminescence properties, large window of fluorescence lifetimes (1 ns−1 μs), ultrasmall size (<2 nm), good biocompatibility, and specific ability as X-ray photosensitizers. Here, we investigated an attractive method that uses fusogenic liposomes to deliver gold nanoclusters into EVs. This approach guarantees the preservation of the EVs membrane without any breakage, thus maintaining compartmental integrity. Different lipid compositions of liposomes preloaded with AuNCs were selected to interact electrostatically with human EVs and compared in terms of fusion efficiency. The mixture of liposomes and EVs results in membrane mixing as demonstrated by FRET experiments and fusion revealed by flux cytometry and cryo-TEM. The resulting fused EVs exhibit typical fluorescence of the AuNCs together with an increased size in agreement with fusion. Moreover, the fusion events in mixtures of EVs and AuNCs preloaded liposomes were analyzed by using cryo-electron microscopy. Finally, the ratio of released AuNCs during the fusion between the fusogenic liposomes and the EVs was estimated to be less than 20 mol % by Au titration using ICP spectroscopy.

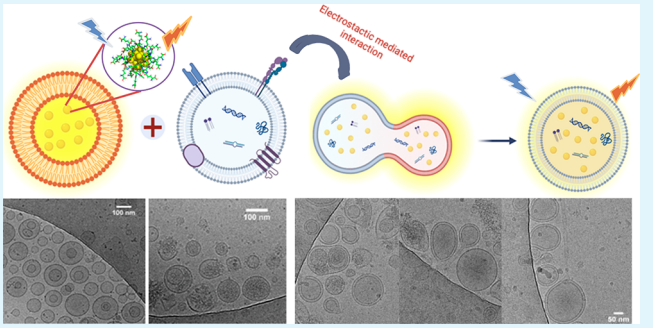

KEYWORDS: *extracellular vesicles, fusion, liposomes, gold nanoclusters, luminescence*

INTRODUCTION

Biological fluids encompass a large variety of extracellular vesicles (EVs), heterogeneous in morphology, size, and content with distinct outcomes for recipient cells.[1−3] EVs are membrane compartments ranging from 30 to 500 nm in diameter loaded with cargo biomarkers such as proteins, lipids, nucleic acids (RNA, DNA[4,5]), and metabolites, reflecting the cell of origin, and are implicated in intercellular communication and regulation.[6] The sorting and the separation of EV subpopulations according to their size remain very challenging, and currently, there is not a simple way to discriminate and sort EVs according to their intravesicular content without disruption.[7] Current methods require time-consuming ultracentrifugation steps and/or magnetic immunocapture that might alter the physical integrity of EVs and modify their heterogeneity. Furthermore, the analysis of their contents requires bulk lysis of the vesicle membrane to extract and purify contained biomolecules (proteins, micro-RNA, or DNA)[8] prior to their analysis, so that information on their distribution at the single vesicle level is irremediably lost. Because of the low abundance of the contained biomolecule cargo in EVs, typically in the femto- to nanomolar ranges), a sensitive and reliable strategy for exosomal biomolecule detection and sorting is highly desirable. In this view, EVs labeled with luminescent nanoprobes could serve as drug delivery vehicles[9] or as therapeutics.[5,10] In the literature alternative efficient methods are described for fluorescent labeling of the EV membrane but not EV intraluminal content by keeping their integrity.[11]

The choice of luminescent gold nanoclusters for probing and labeling the aqueous compartments of EVs is strongly dictated

Received: February 13, 2024
Revised: April 9, 2024
Accepted: April 10, 2024
Published: April 16, 2024

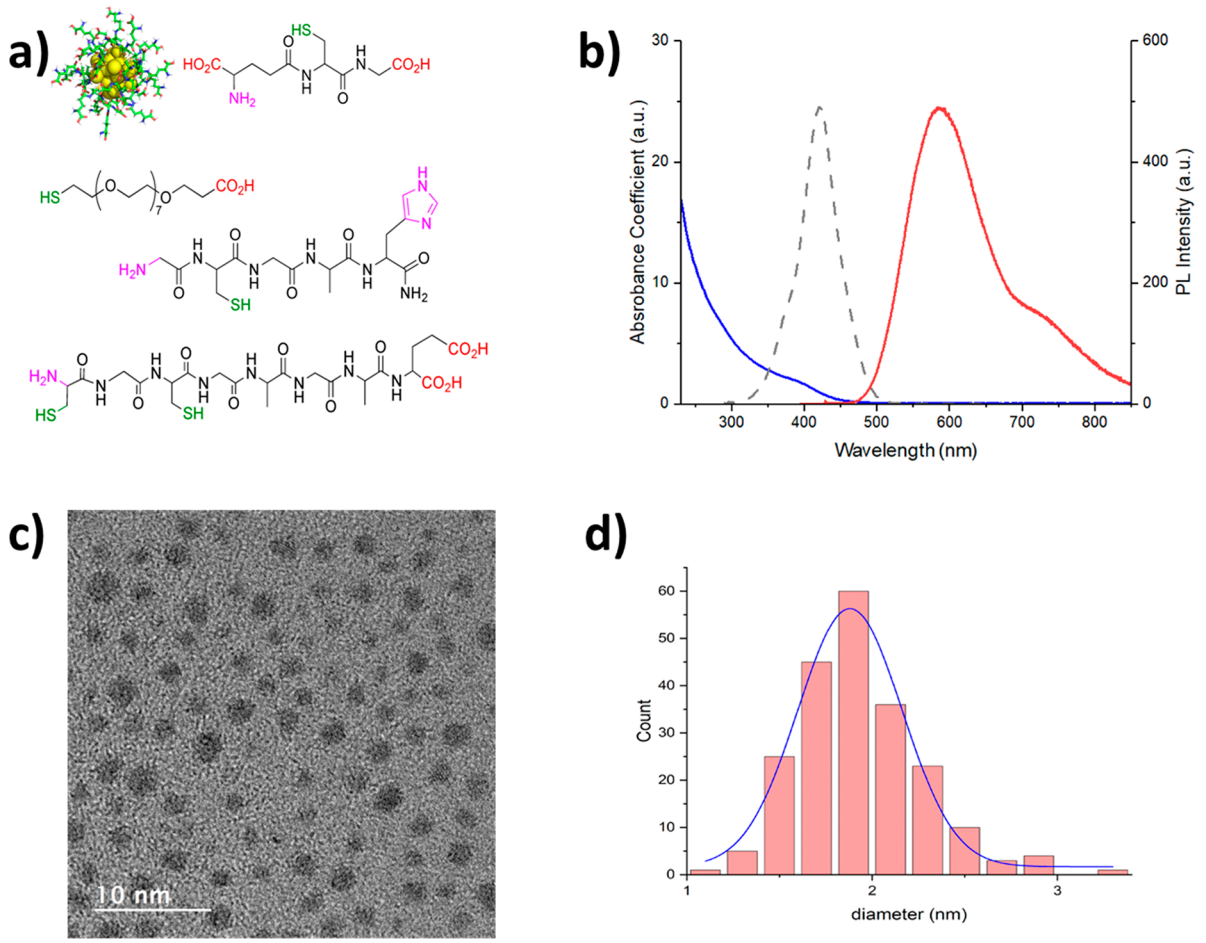

Figure 1. (a) Schematic view of gold nanocluster (AuNCs) and chemical structures of the PEGylated thiol (HS-PEG) and peptide ligands (GCGAH-NH_2 and CGCGAGAE) used to replace the glutathione ligand (GSH). (b) Optical properties of the AuNCs grafted with GSH: absorption spectrum (blue line), excitation spectrum (maximum at 445 nm, gray line), and emission spectrum (maximum at 632 nm, red line) with an excitation wavelength at 445 nm. (c) Typical HRTEM image of the AuNCs and (d) corresponding size distribution extracted from 212 AuNCs nanoclusters (mean diameter 1.9 ± 0.3 nm). The ionizable acid and amine groups in the peptides structures are marked respectively in red (negative) and in pink (positive); the thiol groups acting as Au surface anchors are marked in green.

by their specific luminescent properties due to their ultrasmall size.[12−14] Furthermore, in contrast to organic dyes, which tend to suffer from photobleaching, AuNCs present a high photostability, making labeling more reliable and long-lasting. With regard to their emission, they present not only a luminescence process correlated directly to the number of core gold atoms as expected from quantum confinement effect but also a luminescence related to the interaction between surface Au atoms with long lifetime.[15,16] This second deexcitation process attributed to energy transfer between the ligand and the surface gold atoms also makes them sensitive to the environment. The reactivity of Au(III) salts and the easy Au surface chemistry make them attractive to prepare bioactivated Au nanoprobes sensitive to the environment for biosensing and bioimaging.[17]

All the active EV loading methods[18] such as electroporation, extrusion, or freeze−thaw cycling[19,20] involve breaking and then rebuilding the bilayer membrane to offer a window of opportunity for small drugs encapsulation such as doxorubicin.[21] These strategies are hardly applicable to nanoparticles because of their size.[22,23] Unlike larger particles such as quantum dots, AuNCs pass the kidney barrier and can be easily eliminated from the body by an efficient clearance.[13] The ultrasmall size of AuNCs allows for more effective and less invasive labeling of EVs, preserving their integrity and functionality. They have been previously combined to EVs to form large multilamellar structures resulting from lipid rearrangement with disruption of the aqueous compartment.[24,25] An attractive way that, in principle, may avoid the membrane destabilization and loss of the cargo is based on liposome fusion.[26] In this approach liposomes composed of fusogenic lipids are incubated with EVs to merge their cargo.[27,28] In comparison to other fluorescent dyes such as organic dyes or quantum dots, AuNCs present better biocompatibility, reducing the potential associated long-term toxic effects. In addition, fusion-mediated loading of EVs with fluorescent organic dyes is less appropriate because of their easier release due to their molecular size and also the difficulty to titrate the encapsulation yield. In the case of AuNC, the Au concentration can be easily detected by inductively coupled plasma (ICP) atomic emission spectroscopy. The use of highly luminescent quantum dots failed because they are too big to be efficiently encapsulated in liposomes prepared by extrusion. These characteristics make AuNCs particularly suitable for labeling EVs, allowing not only identification but also potential sorting based on specific luminescent content, thus bringing significant improvements in terms of diagnosis and targeted therapies.

https://doi.org/10.1021/acsami.4c02445
ACS Appl. Mater. Interfaces 2024, 16, 21643−21652

Table 1. Mean Hydrodynamic Diameter Estimated from DLS (D_h) and ζ-Potential Values of the Peptide-Grafted AuNCs Aqueous Suspensions Obtained in PBS Buffer (pH 7.2)

peptide	GSH	GCGAH	CGCGAGAE	HS-PEG
D_h (nm)	3.6 ± 0.2	4.8 ± 0.6	4.0 ± 0.5	5.8 ± 0.8
ζ-potential (mV)	−12.3 ± 4.5	−7.7 ± 2.6	−12.3 ± 3.3	−12.1 ± 2.6

Our strategy aims to use fusogenic liposomes in order to deliver luminescent nanoprobes into the EVs content by keeping the integrity of the membrane compartment. The fusion process between PEGylated liposomes and EVs has been clearly demonstrated.[27] Indeed, liposomes are able to fuse in the presence of PEG, a well-known fusogenic agent.[29−31] This small hydrophilic polymer destabilizes the water molecules in the hydration layer of the membrane, enabling them to be brought into contact for adhesion, a necessary preliminary step to pore opening during fusion.[19,32,33] Another approach consists in using long-range electrostatic attractive interactions, which have been shown to be efficient to promote adhesion.[34] Both approaches can be advantageously combined to balance the energy cost of the fusion process and to reinforce its selectivity. Finally, positive ionizable liposomes containing both PEGylated lipids and cationic lipids such as 1,2-dioleoyl-3-dimethylammonium propane (DODAP), which is less toxic than 1,2-dioleoyl-3-trimethylammonium propane (DOTAP), were shown to be particularly efficient fusogenic drug delivery systems (DDS) and gave rise to many recent developments of lipid nanoparticles.[35,36]

Here, our strategy is to develop an efficient method to encapsulate AuNCs into fusogenic liposomes. Unlike larger nanoparticles such as quantum dots, gold nanoclusters, thanks to their ultrasmall size (less than 2 nm), can be loaded inside liposomes without causing the disruption of the membrane or even changing the compartment integrity.[25] The fusion between liposomes of various lipid compositions preloaded with gold nanoclusters and EVs was investigated to optimize the loading efficiency in gold. The fusion process was analyzed at a nanometric resolution by using cryo-electron microscopy. Finally, the encapsulation efficiency in EVs was quantified by gold titration with ICP atomic emission spectroscopy. These results provide new insights for EVs lumen labeling and potentially EVs sorting according to their content, which represent major breakthroughs for both diagnostic and therapeutic applications.

RESULTS AND DISCUSSION

Gold nanoclusters grafted with peptides of different surface charges (positive or negative) were prepared to minimize possible interaction with the lipid membranes and facilitate their encapsulation into liposomes. First, gluthathione nanoclusters were obtained with an emission intensity maximum at 600 nm corresponding to stable GSH Au_{25} nanoclusters. A chemical platform of peptide ligands was designed for AuNCs synthesis to obtain different charged AuNCs. Short peptides bearing a cysteine and an ionizable terminal amino acid, either positively charged histidine (GCGAH-NH_2) or negatively charged aspartic acid (CGCGAGAE), as well as a PEGylated thiol (HS-PEG) were selected to be grafted onto red emitting gold nanoclusters (AuNCs) (see Figure 1). The hydrophilicity of the ligands assures colloidal stability, while the sulfur to gold affinity is strong enough to stabilize the organic layer of ligands and the luminescence of gold nanoclusters. The AuNCs are initially prepared by reduction of an aqueous $HAuCl_4$ solution with the glutathione ligand, which is replaced with the peptide (GCGAH-NH_2 and CGCGAGAE) or HS-PEG in excess.

The hydrodynamic diameter estimated from DLS measurement is around 4 ± 2 nm (see Figure S1), significantly higher than the gold core diameter of the AuNCs found to be 1.9 ± 0.3 nm from transmission electron microscopy. Their surface charge changes according to the ionization state of the peptides, as illustrated from zeta-potential values (see Table 1).

After GSH ligand exchange and removal of the peptide excess by ultrafiltration, the FTIR spectra of lyophilized AuNCs were collected. The FTIR spectra with peptides in Figure S2 show peaks at about 1540 and 1650 cm^{-1}, which correspond to the N−H bond bending and the stretching of the carbonyl group of the amide, respectively. The FTIR spectrum of HS-PEG exhibits the characteristic bands of HS-PEG ligands in the 1200−1000 cm^{-1} range. The spectrum of the GSH AuNCs has a broad peak at ∼3400 cm^{-1}, which corresponds to one or more OH-free bonds. Furthermore, the presence in all the spectra of the peak at about 1230 cm^{-1} is referred to the bond between gold and sulfur.[37] After ligand exchange, there were no significant changes in the emission wavelength, while the luminescence intensity of peptide AuNCs was enhanced for all three compounds in comparison to GSH AuNCs (see Figures S3 and S4). This enhancement aligns with the expected outcome of increased ligand-to-metal charge transfer, especially when the gold nanocluster surface is saturated with the ligand.[38] The synthesis yield of the AuNCs surface exchange by using different peptides was estimated through gold titration by ICP mass spectroscopy. As shown in Table 2, the gold yield were found to be 59−83 mol % in the AuNCs after ligand exchange depending on the chemical nature of the ligand.

Table 2. Synthesis Yields of the AuNCs Surface's Exchange and Encapsulation Yields into Liposomes (LUV) Estimated from Gold Concentrations Measured by ICP Atomic Emission Spectroscopy

ligand	peptide AuNCs yield (mol %)	encapsulation yield (mol %) in LUV
CGCGAGAE	69	42
$GCGAH_{NH2}$	83	26
HS-PEG	59	29

Exosome-like-sized liposomes were then prepared by the extrusion method to obtain large unilamellar liposomes with a well-defined diameter (see Figure 2a).[39] The lipid mixture was first dried to give a film which was then hydrated and swollen in the presence of a suspension containing luminescent peptide−gold nanoclusters to form multilamellar vesicles by five freeze/thaw cycles as previously described.[39] To evaluate the efficiency of the peptide−Au NCs preparation and encapsulation process, after LUV purification, the amount of gold was estimated by ICP mass spectroscopy, and it was found to be from 26 to 42 mol %, depending on the peptide grafted (see Table 2).

https://doi.org/10.1021/acsami.4c02445
ACS Appl. Mater. Interfaces 2024, 16, 21643−21652

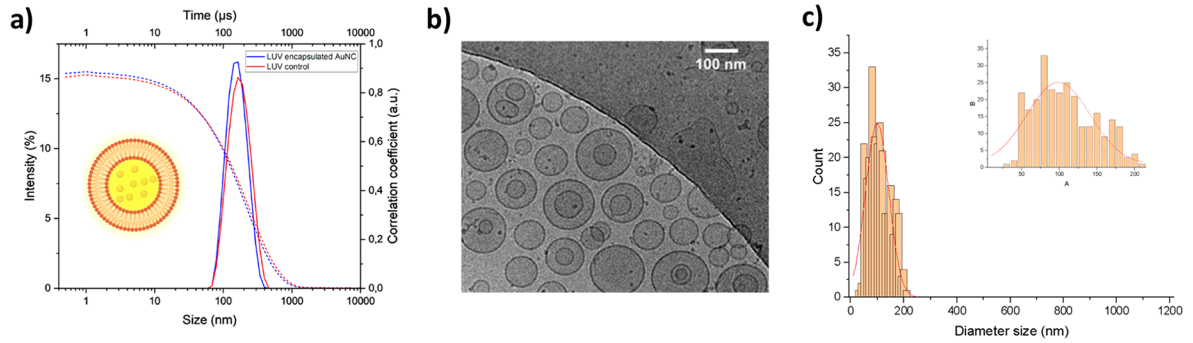

Figure 2. Characterization of AuNCs preloaded fusogenic liposomes. (a) DLS correlograms and light scattering intensity histograms of AuNCs (grafted here with GCGAH) preloaded liposomes composed of a 85:10:5 DOPC:DODAP:PEG2000-DOPE mixture. (b) Typical cryo-TEM image after elimination of the nanocluster excess by size exclusion chromatography. (c) Corresponding size histogram extracted from 322 vesicles observed by cryo-TEM with a mean diameter of 116 ± 45 nm. The inset highlights a size distribution from 50 to 200 nm without the presence of bigger aggregates.

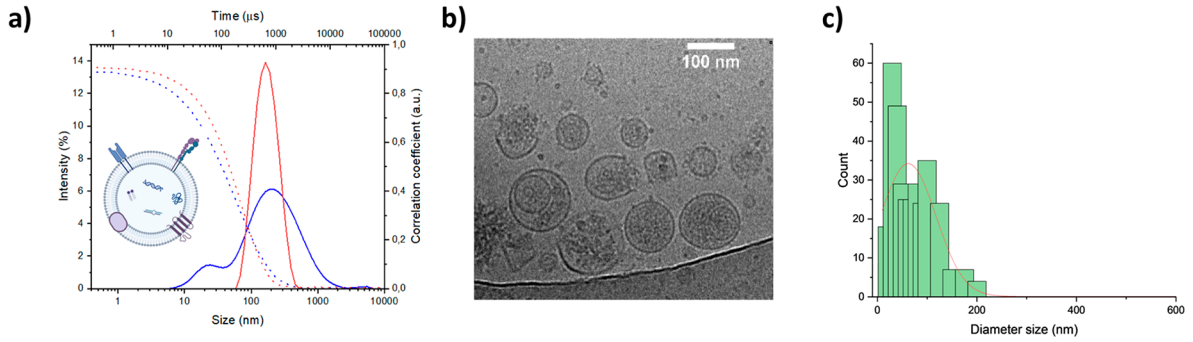

Figure 3. Characterization of EVs from a human seminal fluid. (a) Dynamic light scattering correlogram and intensity size profile of EVs extracted from seminal fluid before and after ultracentrifugation (crude EVs in blue and purified EVs in red). (b) Typical cryo-TEM image of purified EVs. (c) Corresponding size histogram extracted from 358 vesicles observed by cryo-TEM with a mean diameter of 74 ± 20 nm.

As expected from the 200 nm pore size used for extrusion, the liposome hydrodynamical diameter is around 100−200 nm, which is confirmed from the DLS correlograms and histograms (Figure 2b). As shown in Figure 2c, the liposomes appear mostly monolamellar or bilamellar in the cryo-TEM images. The mean diameter of the LUV preloaded with GCGAH-AuNCs obtained by cryo-TEM was found to be 116 ± 45 nm (Figure 2d). The LUV preloaded with negatively charged HS-PEG AuNCs were also analyzed by DLS and cryoTEM, giving mostly unilamellar vesicles with a mean diameter at 158 ± 45 nm (Figure S5).

EVs extracted from human reproductive fluids were selected as a target because of their huge concentration and their relevance for diagnosis in liquid biopsies for infertility related pathologies. The detection of their content is a great challenge because there is currently no nondisruptive methods to analyze the EVs cargo. Particularly, the *in situ* detection of overexpressed miRNAs involved in pathological developments could serve as early diagnosis factors. Furthermore, the detection of specific miRNAs of biological interest may potentially benefit reducing resistance to chemotherapeutic therapies.

The male seminal fluid and female follicular fluid are reproductive fluid containing both a high concentrated and heterogeneous population of EVs[11] that were purified by ultracentrifugation according to the literature.[41] These EVs-rich fluids are good models for the study of human vesicle interactions. The EVs extracted from seminal male fluid show a higher concentration and lower polydispersity in size than the vesicles extracted from the follicular fluid. For this reason, most of our experiments were performed on EVs extracted from seminal male fluids. The mean hydrodynamic diameter of these EVs measured by DLS is around 74 ± 20 nm, as shown in Figure 3.

Different compositions of the LUV preloaded with gold nanoclusters were first investigated to fuse with human EVs from seminal plasma EVs. Lipids having a negative spontaneous curvature (such as PE or PEG_{2000}-PE) or cholesterol were introduced in the liposome composition because of their ability to go from a lamellar to an hexagonal phase, a transition required in the local rearrangement occurring during the fusion (see Table S1). The ability of liposomes to interact with EVs has been evaluated by using a classical fluorescence lipid mixing test based on FRET change between two donor (NBD-PE) and acceptor (Rhodamine-PE) fluorescent lipids depending on their mean distance in the vesicle membrane.[42−45] As a fusogenic agent, a poly(ethylene glycol) polymer was first incubated for 2 h in the presence of a (1:1) mixture containing (NDB/Rh) LUV and EVs. Increasing amounts of PEG were added, and the fusion ratio was estimated from the FRET decrease between the donor and the acceptor initially present in the liposomes (see Figure S6). The most efficient PEG concentration to induce fusion was found to be 25 mol %, in agreement with the literature.[27] Nevertheless, the viscosity of the 25% PEG solution in the cytometer microfluidic system makes it difficult to regenerate the capillary between two successive samples. Furthermore, fusion can occur between liposomes as well as liposomes/EVs. For these reasons, we decided to introduce an attractive

https://doi.org/10.1021/acsami.4c02445
ACS Appl. Mater. Interfaces 2024, 16, 21643−21652

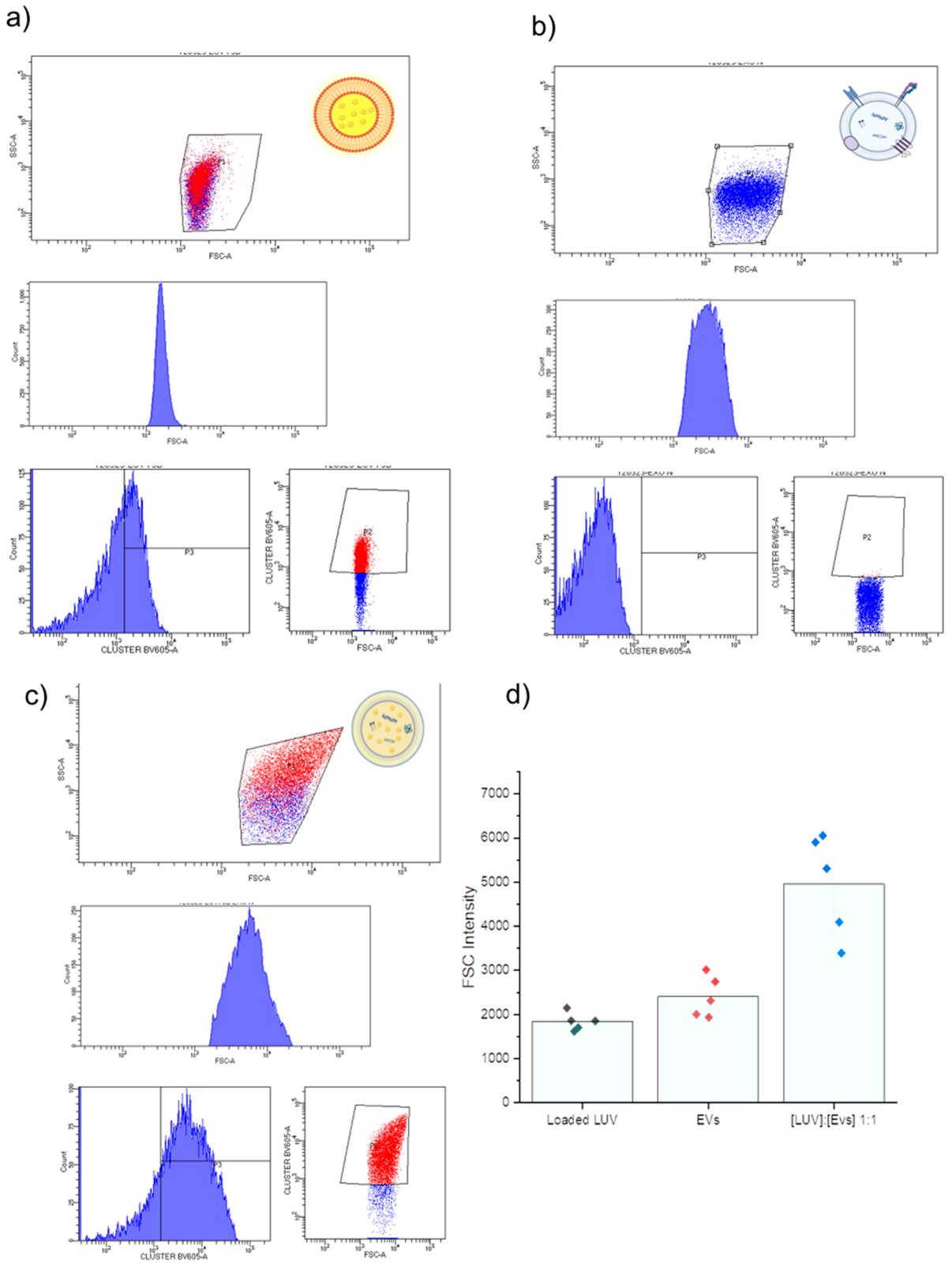

Figure 4. Flux cytometry measurements showing the size and fluorescence evolution of the (EV:LUV) mixture. Scattering intensity (denoted FSC-A) and fluorescence intensity at 605 nm (denoted ClusterBV605 nm) evolution of (a) AuNCs preloaded liposomes, (b) human semen EVs, and (c) 1:1 EV:LUV mixture after 2 h of incubation. (d) Fluorescence intensity at 605 nm of (a−c) for five cytometry fusion assays showing the reproducibility of the size increase.

electrostatic interaction. Different ratios between EVs and cationic liposomes were investigated to optimize fusion efficiency and to determine the size increase as they interact through electrostatic interaction (see Figure S7). The best liposomes/EVs ratio was found to be the 1:1 molar mixture. The composition of the liposomes was then optimized.

https://doi.org/10.1021/acsami.4c02445
ACS Appl. Mater. Interfaces 2024, 16, 21643−21652

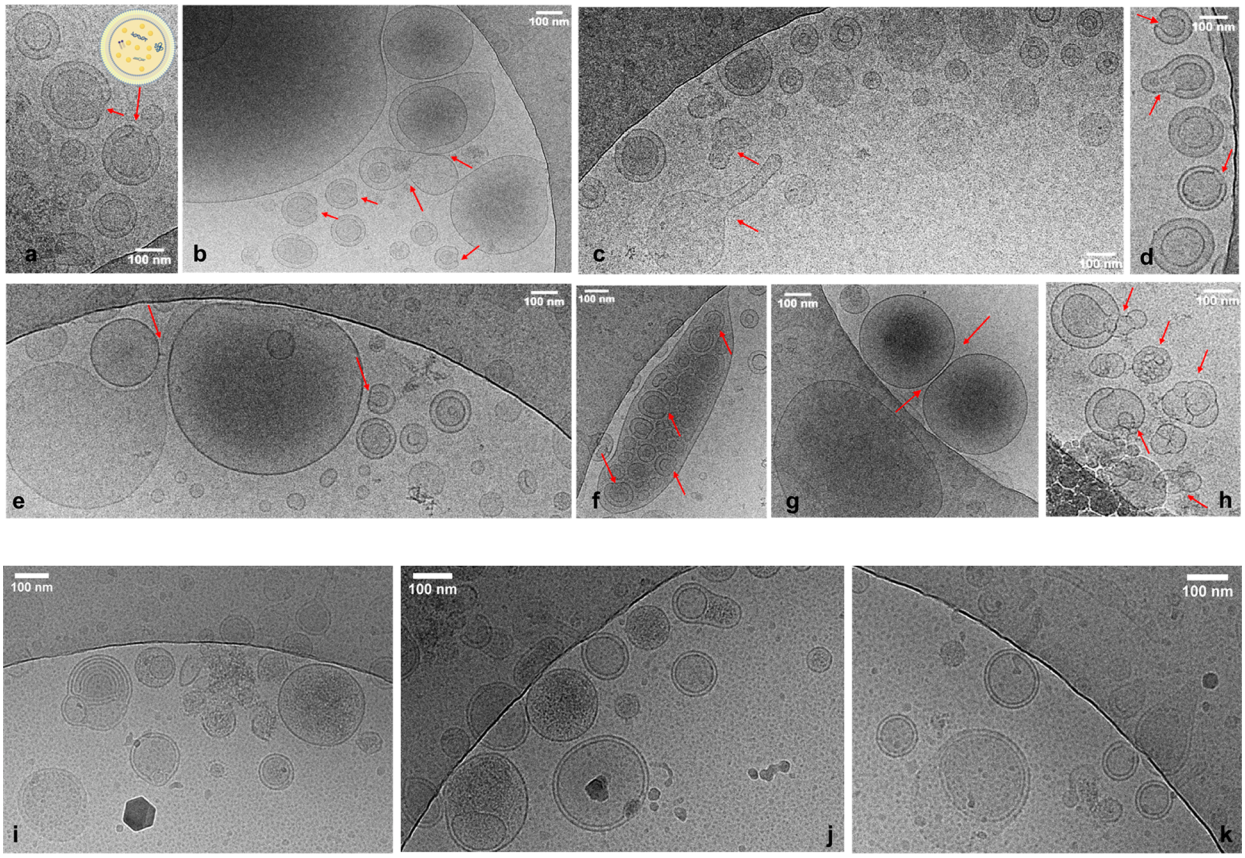

Figure 5. Cryo-TEM imaging of the 1:1EV:LUV mixture revealing fusion intermediates (see red narrows) in a 1:1 EVs:LUVmixture after 2 h of incubation (a–h) and after 24 h of incubation (i–k).

DODAP, which replaced DOTAP, is an ionizable lipid less toxic than the cationic analogue[46] and was introduced in the lipid compositions (see Table S1 and Figure S8). This lipid is also currently used for miRNA or lipid nanoparticle drug delivery and DNA transfection.[35,36] Thus, liposomes preloaded with GCGAH or HS-PEG were prepared from a mixture of DODAP/DOPC/PE-PEG5000 (10:85:5 mol %) and incubated for 2 or 24 h in the presence of purified EVs (see Figure S9). We selected positively ionizable GCGAH and negatively ionizable HS-PEG to investigate the effect of a possible electrostatic interaction with the liposome membrane during the extrusion process. No destabilization of the liposome membrane was observed whatever the ionizable peptide used (Figure 2 and Figure S5).

Fluorescent detection of loaded AuNCs in the EVs by cytometry permits us also to evidence the EVs/liposome fusion by following the increasing size and fluorescence. Cytometry measurements clearly show an increase in EVs size and fluorescence attributed to the gold emission intensity at 620 nm after 2 h of incubation (see Figure 4). As shown in Figure S9, the best condition to improve the fusion events corresponds to the (1:1) equimolar ratio as determined by NTA. Furthermore, the NTA analysis clearly shows that due to the fusion event, the residual AuNCs concentration in solution decreases dramatically. The efficiency of the fusogenic liposomes to fuse with EVs extracted from female follicular fluid was also tested. Also in this case, the cytometry assay results show an increase in size and fluorescence of the vesicles after 2 h of incubation (see Figure S10).

To more precisely investigate the liposome/EVs interaction, as well as the morphology and size change in the vesicles population, cryo-TEM imaging on the 1:1 mixture was performed. Membrane fusion intermediate states include (i) close contact between the two bilayers, (ii) adhesion and hemifusion with lipid mixing, (iii) opening of a pore to allow the content mixing, (iv) expansion of the fusion pore, and (v) fused vesicles resulting from the pore closing.[34] EVs incubated with liposomes (LUV) for 2 h showed remarkably very large vesicles of 200–500 nm resulting from successive fusions (see Figure 5a–h). After 24 h of incubation, the vesicles' concentration appears to be lower, and vesicles of bigger size are observed. The diameter size histograms clearly show a significant size increase of the initial populations as shown in Figure 6a–c within 2 h. For a long time (24 h) of incubation, the increase in size is slightly higher, but more vesicle rupture events are also observed, so that the optimal time in terms of fusion efficiency appears to be 2 h (see Figure 5i–k). The more detailed analysis of the morphological profiles permits classification of the different fusion intermediate states (Figure 6d). A high ratio of fusion intermediates was obtained as shown in Figure 6d including a hemifusion state (5%), initial pore (6%), expanded pore (6%), and fused vesicles including intermediate fusion (28%) and fusion event (56%). In the case of LUV preloaded with HS-PEG AuNC interacting with EVs, fusion intermediates were also evidenced and classified from cryo-TEM images (Figure S11). The fusion process occurs in both cases for GCGAH and HS-PEG peptides used for coating AuNCs. Hence, the charge of the coating peptide used for preloading the LUVs appears not to affect the fusion process.

https://doi.org/10.1021/acsami.4c02445
ACS Appl. Mater. Interfaces 2024, 16, 21643–21652

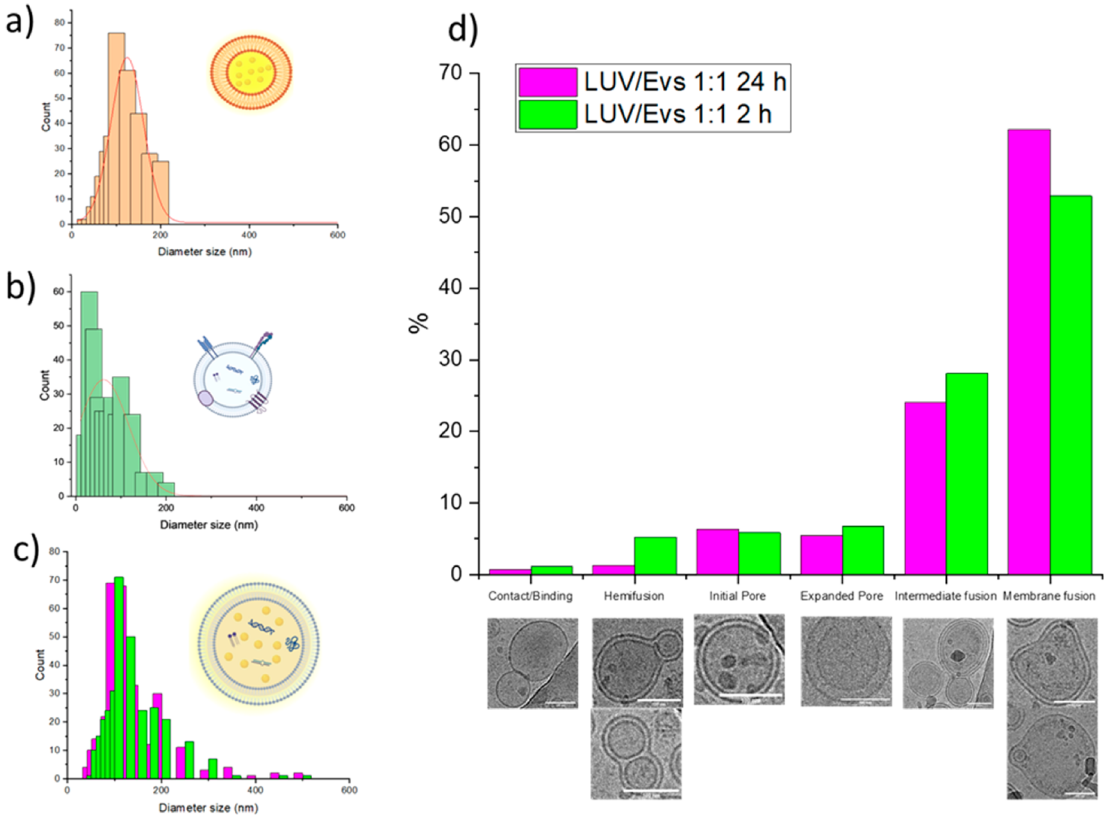

Figure 6. Size histograms extracted from the cryo-TEM imaging of (a) pure LUV, (b) human EVs, and (c) 1:1 LUV:EVs mixture after 2 h (green) with a mean diameter of 175 ± 65 nm and 24 h (pink) with a mean diameter of 138 ± 74 nm. (d) Corresponding histogram showing the frequency number of those intermediates for the EVs:LUV mixture and canonical fusion intermediates including contact/binding, hemifusion, initial pore, expanded pore, and membrane fusion. The scale bar represents 100 nm.

Finally, fused vesicles resulting from the interaction between EVs and fusogenic liposomes preloaded with GCGAH AuNC were separated from the released AuNCs during the fusion by size exclusion chromatography and characterized by flux cytometry and fluorescence spectroscopy (Figure S12). The first fraction corresponds to the vesicles including the fused vesicles and the possible residual liposomes. The second fraction does not contain any vesicle but appears to be slightly fluorescent at 620 nm. This fraction is attributed to the AuNCs released during the fusion events. To quantify the efficiency of the EV labeling, ICP titrations were performed to give a quantitative estimation of the gold concentration in each fraction of the EVs:LUV mixture (Table 3), giving access to the free AuNCs detected by fluorescence after fusion. The total gold concentration before the purification of the EVs:LUV mixture was considered as the reference (100 mol %). As shown in Table 3, the gold release (fraction 2) during the fusion represents only 17 mol % of the total gold amount present in the EVs:LUV mixture, showing the efficiency of the fusion process to encapsulate the AuNCs into EVs without membrane rupture. As a control the gold concentration was also quantified for the pure LUV loaded with the AuNC. 39 mol % of total gold amount introduced during the liposome preparation was detected just after extrusion and 29 mol % in the purified LUV loaded with AuNCs after purification on SEC.

Table 3. Gold Concentrations Were Estimated from ICP Titration during LUV Loading by Extrusion and EV Loading by Fusion with Liposomes[a]

LUV loading with AuNC by extrusion		EV loading with AuNC by fusion	
purified AuNC	4.710 mM (100 mol %)	EVs:LUV mixture	0.666 mM (100 mol %)
LUV after extrusion	1.826 mM (39 mol %)	fused vesicles (f1)	0.551 mM (83 mol %)
purified LUV	1.354 mM (29 mol %)	AuNCs release (f2)	0.114 mM (17 mol %)

[a]Fused vesicles and AuNC release were attributed respectively to fraction 1 (noted f1) and fraction 2 (f2) obtained by SEC purification of the EVs:LUV) mixture after 2 h of incubation.

CONCLUSION

We have introduced an innovative approach to labeling extracellular vesicles (EVs) using luminescent gold nanoclusters (AuNCs), highlighting considerable potential in both early diagnostics and improved drug delivery. This technique, which preserves the integrity of EV membranes, paves the way for future applications for the analysis of EV contents and targeted drug delivery, offering significant advantages over conventional methods.

The interaction of fusogenic liposomes loaded with AuNCs and EVs results in an efficient labeling of these EVs with luminescent nanoclusters. The composition of the membrane was optimized to improve the fusion properties of the liposomes. The incorporation of both cationic ionizable DODAP and PEG−PE in the lipid composition, instead of fusogenic PEG additive, was particularly adapted to facilitate

https://doi.org/10.1021/acsami.4c02445
ACS Appl. Mater. Interfaces 2024, 16, 21643−21652

fusion. This fusion process was easily detected by flux cytometry thanks to the AuNCs fluorescence, while concurrently preventing viscosity elevation due to PEG addition. The mixture of liposomes and EVs results in lipid exchange, as demonstrated by FRET experiments and increased size revealed by flux cytometry. The fused vesicles exhibit a typical fluorescence of the AuNCs together with an increased size, in agreement with the expected size of the fused exosomes. The fusion intermediates in mixtures of EVs and AuNCs preloaded liposomes are also clearly visualized and analyzed by using cryo-electron microscopy. In addition, the resulting fused vesicles are successfully isolated by size exclusion chromatography and fluorescently labeled with AuNC. Less than 20% of the cluster is released after mixing the two species according to Au titration performed by ICP atomic emission spectroscopy. Hence, here we show the efficiency of the fusion process to encapsulate the AuNCs into human EVs extracted from EVs-rich human reproductive fluids without membrane disruption.

These results provide new insights for EVs lumen labeling and potentially EVs sorting according to their content, which would represent a major breakthrough for both diagnostic and therapeutic applications. In terms of applications, our method is not limited exclusively to labeling but significantly extends to EVs sorting. By using the specific luminescence of AuNCs, separation and identification of different populations of EVs based on their contents could be facilitated, thus improving the early diagnosis and precision of treatment of various medical conditions. This is particularly relevant in areas where the precise sorting of EVs can have direct impacts, such as in the identification of biomarkers for diseases or in the development of targeted therapies. Future prospects of this research include expanding the use of labeled EVs in clinical settings for the early diagnosis and treatment of diseases, particularly in those with limited diagnostic and therapeutic options. Furthermore, the use of EVs taken directly from patients highlights the immediate applicability and clinical relevance of our work. This innovative technology paves the way to future development in the field of personalized medicine and targeted drug delivery.

EXPERIMENTAL PART

Materials. Glutathione (GSH) and $HAuCl_4 \cdot 3H_2O$ were purchased from Sigma-Aldrich. DOPC, DOPE, DODAP, DOTAP, PEG_{2000}-PE, Rhodamine-PE, and *N*-(7-nitrobenz-2-oxa-1,3-diazol-4-yl)-PE (NBD-PE) lipids were purchased from Avanti Polar Lipids. The ultrafiltration devices were Amicon Ultra devices with 10000 MWCO (10 kDa) and 3000 MWCO (3 kDa) cutoff. All solutions were prepared by using Milli-Q water.

Methods. *FTIR Spectroscopy.* The measurements were performed with a JASCO FT/IR-4600 by ATR powder diffusion.

Absorption Spectroscopy. The UV−vis absorption spectra were recorded by Nanodrop One (Thermo Scientific) using a drop of 2 μL of each sample.

Fluorescence Measurements. All fluorescence spectra and 2D maps were performed by a Horiba instrument (Jobin Yvon Duetta).

DLS Spectroscopy. The hydrodynamic diameters of the various colloidal suspensions were measured by a Zetasizer Nano-ZS (MALVERN Instrument) with an angle of 173° at 25 °C. The data were analyzed with Zetasizer software.

Flux Cytometry. The size and fluorescence of AuNCs and EVs were performed on a LSR Fortessa X-20 (BD Biosciences) with five lasers (355, 405, 488, 561, and 640 nm). FACS Diva software version 8 (BD) was used for collecting data.

Transmission Electron Microscopy (TEM). TEM analyses were performed with a JEOL 2100 transmission electron microscope operated at 200 kV supplied with an UltraScan 1000XP CCD camera. For sample preparation, 300 mesh copper grids were placed for 1 min on top of a 40 μL sample droplet and dried with paper. Particle sizes were determined from TEM micrographs using DigitalMicrograph GMS3 software.

Cryo-TEM. Vitrification of vesicles was performed using an automatic plunge freezer (EMGP, Leica) at controlled humidity and temperature.[47] The samples were deposited onto glow discharged electron microscope grids, followed by blotting and vitrification by rapid freezing in liquid ethane. Grids were transferred to a single axis cryo holder (model 626, Gatan) and observed using a 200 kV electron microscope (Tecnai G2T20 Sphera, FEI) equipped with a 4K × 4K CCD camera (XF416, TVIPS). Micrographs were acquired under small electron doses using the camera in binning mode 1 and at a nominal magnification of 25000×.

NTA Measurements. Before nanoparticle tracking analysis (NTA), EVs, LUV, and Mixture samples were diluted in sterile PBS. NTA used a NanoSight LM14 instrument (Malvern Instruments, Malvern, UK) to measure the size distribution and vesicle concentration. A 405 nm laser beam is employed. At 25 °C, five 30 s recordings were recorded for each sample. The NanoSight NTA 3.1 software (Malvern, UK) was used to analyze the videos with a detection threshold of 5. For every sample, the results displayed match the average of the five recorded videos. After that, the distributions and concentrations were standardized.

Zetametry. The ζ-potential measurements were performed using the Zetasizer ZEN3600 (Malvern Instruments) equipped with a He−Ne laser source (λ = 633 nm). The solutions of the vesicles were loaded into disposable folded capillary cells (Zeta Cell, DTS 1060), and data were collected at 25 °C.

Gold Nanoclusters Synthesis. AuNCs were synthesized by adding in a 100 mL flask, 33.6 mL of Milli-Q water and 2 and 4 mL of a 50 mM solution of GSH; then, 4 mL of a 20 mM solution of $HAuCl_4$ was added under stirring, and the solution was immediately moved on a hot plate set at 120 °C to get a reflux. The as-obtained solution was left to stir for 4 h. After this time, the solution was allowed to cool at room temperature and transferred in a brown bottle to preserve it from sunlight. All of the labware was previously washed with aqua regia.

Gold Nanoclusters Ligand Exchange. 4 mL of GSH−AuNCs was put into a vial, and 1.56 mL of a 20 mM solution of the needed ligand was added. The obtained mixture was left to incubate overnight. To remove the GSH and the ligand excess, after the incubation time, the solution was filtered using Amicon filter of 3 kDa at 7100 rcf for 20 min; the solution retained by the filter containing the purified clusters was collected and analyzed by DLS, fluorescence, UV, and TEM microscopy.

EVs Purification. The seminal plasma from human semen without spermatozoa or from the follicular fluid was transferred into a new Falcon tube and centrifuged for 30 min at 3000*g* and 4 °C; then, the supernatant (25−30 mL) was centrifuged for 35 min at 10000*g* and 4 °C in a new Falcon tube. The obtained supernatant (25−30 mL) was again centrifuged for 60 min at 110000*g* and 4 °C; the obtained pellet was resuspended in PBS (p H 7.2) and ultracentrifuged again using the same settings as before. The final pellet containing EVs was resuspended in 800 μL of PBS, divided in 8 aliquots, and stored at −80 °C.

LUV Synthesis and Loading with AuNCs. The lipid mixture in chloroform was first prepared from a stock solution of lipids in chloroform according to the desired composition. After solvent evaporation by using a rotavapor, the lipid film is then rehydrated with an aqueous AuNCs suspension to load them with the nanoclusters and submit to 5 freeze−thaw cycles, each cycle providing an incubation of 50 s in liquid nitrogen followed by 5 min in a 45 °C water bath. At the end of these cycles, the resulting MLV suspension is extruded 10 times using a semiautomatic extruder with a 0.2 μm pore-sized carbonate filter.

https://doi.org/10.1021/acsami.4c02445
ACS Appl. Mater. Interfaces 2024, 16, 21643−21652

■ ASSOCIATED CONTENT

Supporting Information

The Supporting Information is available free of charge at https://pubs.acs.org/doi/10.1021/acsami.4c02445.

Characterization of AuNCs grafted with different ligands: DLS spectroscopy correlograms and size histograms (Figure S1); FTIR spectra (Figure S2); absorbance, fluorescence, emission, and excitation spectra of the different AuNCs (Figure S3); emission-excitation mapping (Figure S4); characterization of fusogenic liposomes preloaded with HS-PEG AuNC (Figure S5); Table S1 summarizes the different lipid compositions used for fusogenic liposomes; FRET lipid mixing assay by PEG-mediated fusion on 1:1 EV:LUV mixture of AuNC preloaded liposomes and EVs (Figure S6); effect of the EV:LUV ratio (Figure S7) and effect of cholesterol and cationic lipid in the composition of fusogenic liposomes (Figure S8); size evolution of EV:LUV mixtures with different ratios measured by NTA after an incubation time of 2 or 24 h (Figure S9); evidence of fusion with EVs extracted from female follicular fluid followed by flux cytometry (Figure S10); size analysis extracted from cryo-TEM images in the case of the HS-PEG LUV:EV mixture (Figure S11); emission spectra of the two fractions corresponding to fused vesicles and released AuNC after purification of the 1:1 EV:LUV mixture (Figure S12) (DOCX)

■ AUTHOR INFORMATION

Corresponding Author

Valérie Marchi − *Institut des Sciences Chimiques de Rennes ISCR, UMR CNRS 6226, University Rennes, 35042 Rennes, France;* orcid.org/0000-0002-6565-7201; Email: valerie.marchi@univ-rennes.fr

Authors

Ester Butera − *Institut des Sciences Chimiques de Rennes ISCR, UMR CNRS 6226, University Rennes, 35042 Rennes, France; Dipartimento di Scienze Chimiche, Università degli Studi di Catania, Catania 95125, Italy*

Aurelien Dupont − *CNRS, Inserm, BIOSIT—UMS 3480, Univ Rennes, F-35000 Rennes, France*

Alexis Aimé − *CNRS, Inserm, BIOSIT—UMS 3480, Univ Rennes, F-35000 Rennes, France*

Solène Ducarre − *Institut des Sciences Chimiques de Rennes ISCR, UMR CNRS 6226, University Rennes, 35042 Rennes, France; Institut de Recherche en Santé, Environnement et Travail IRSET, F-35000 Rennes, France*

Regina M. Chiechio − *Dipartimento di Fisica e Astronomia, Università di Catania, 95123 Catania, Italy;* orcid.org/0000-0002-6469-3059

Pascale Even-Hernandez − *Institut des Sciences Chimiques de Rennes ISCR, UMR CNRS 6226, University Rennes, 35042 Rennes, France*

Annalinda Contino − *Dipartimento di Scienze Chimiche, Università degli Studi di Catania, Catania 95125, Italy;* orcid.org/0000-0003-2443-9352

Giuseppe Maccarone − *Dipartimento di Scienze Chimiche, Università degli Studi di Catania, Catania 95125, Italy*

Célia Ravel − *Institut de Recherche en Santé, Environnement et Travail IRSET, F-35000 Rennes, France; Centre Hospitalier Universitaire CHU Rennes, Service de Biologie de la Reproduction-CECOS, 35000 Rennes, France*

Complete contact information is available at: https://pubs.acs.org/10.1021/acsami.4c02445

Notes

The authors declare no competing financial interest.

■ ACKNOWLEDGMENTS

We are thankful to the Catania University for the financial support to the PhD fellowship of E.B. and R.M.C. We are thankful to Ligue contre le Cancer and University of Rennes for their financial support and the PhD fellowship of S.D. We are also thanksful to Bertrand Lefeuvre for the technical support in ICP measurements and Gregory Taupier for his technical support in fluorometry experiments and the access to CAPHTER plateform (ScanMat, Rennes University).

■ ABBREVIATIONS

EVs, extracellular vesicles; AuNCs, gold nanoclusters; ICP, inductively coupled plasma; TEM, transmission electron microscopy; NTA, nanoparticle track analysis.

■ REFERENCES

(1) Johnstone, R. M.; Adam, M.; Hammond, J. R.; Orr, L.; Turbide, C. Vesicle Formation during Reticulocyte Maturation. Association of Plasma Membrane Activities with Released Vesicles (Exosomes). *J. Biol. Chem.* **1987**, *262* (19), 9412.

(2) Théry, C.; Amigorena, S.; Raposo, G.; Clayton, A. Isolation and Characterization of Exosomes from Cell Culture Supernatants and Biological Fluids. *Curr. Protoc. Cell Biol.* **2006**, *30*, 3.

(3) Raposo, G.; Stoorvogel, W. Extracellular Vesicles: Exosomes, Microvesicles, and Friends. *J. Cell Biol.* **2013**, *200* (4), 373.

(4) Valadi, H.; Ekström, K.; Bossios, A.; Sjöstrand, M.; Lee, J. J.; Lötvall, J. O. Exosome-Mediated Transfer of MRNAs and MicroRNAs Is a Novel Mechanism of Genetic Exchange between Cells. *Nat. Cell Biol.* **2007**, *9* (6), 654.

(5) Cheng, L.; Hill, A. F. Therapeutically Harnessing Extracellular Vesicles. *Nat. Rev. Drug Discov* **2022**, *21*, 379.

(6) Mathieu, M.; Martin-Jaular, L.; Lavieu, G.; Théry, C. Specificities of Secretion and Uptake of Exosomes and Other Extracellular Vesicles for Cell-to-Cell Communication. *Nat. Cell Biol.* **2019**, *21* (1), 9.

(7) Théry, C.; et al. Minimal Information for Studies of Extracellular Vesicles 2018 (MISEV2018): A Position Statement of the International Society for Extracellular Vesicles and Update of the MISEV2014 Guidelines. *J. Extracell. Vesicles* **2018**, *7* (1), 1535750.

(8) Shahabipour, F.; Barati, N.; Johnston, T. P.; Derosa, G.; Maffioli, P.; Sahebkar, A. Exosomes: Nanoparticulate Tools for RNA Interference and Drug Delivery. *J. Cell. Physiol.* **2017**, *232* (7), 1660.

(9) Herrmann, I. K.; Wood, M. J. A.; Fuhrmann, G. Extracellular Vesicles as a Next-Generation Drug Delivery Platform. *Nat. Nanotechnol.* **2021**, *16* (7), 748.

(10) O'Brien, K.; Breyne, K.; Ughetto, S.; Laurent, L. C.; Breakefield, X. O. RNA Delivery by Extracellular Vesicles in Mammalian Cells and Its Applications. *Nat. Rev. Mol. Cell Biol.* **2020**, *21* (10), 585.

(11) Di, H.; Zeng, E.; Zhang, P.; Liu, X.; Zhang, C.; Yang, J.; Liu, D. General Approach to Engineering Extracellular Vesicles for Biomedical Analysis. *Anal. Chem.* **2019**, *91* (20), 12752.

(12) Zhang, X.-D.; Wu, D.; Shen, X.; Liu, P.-X.; Fan, F.-Y.; Fan, S.-J. In Vivo Renal Clearance, Biodistribution, Toxicity of Gold Nanoclusters. *Biomaterials* **2012**, *33* (18), 4628.

(13) Loynachan, C. N.; Soleimany, A. P.; Dudani, J. S.; Lin, Y.; Najer, A.; Bekdemir, A.; Chen, Q.; Bhatia, S. N.; Stevens, M. M. Renal Clearable Catalytic Gold Nanoclusters for in Vivo Disease Monitoring. *Nat. Nanotechnol.* **2019**, *14* (9), 883.

(14) Zhang, Y.; Zhang, C.; Xu, C.; Wang, X.; Liu, C.; Waterhouse, G. I. N.; Wang, Y.; Yin, H. Ultrasmall Au Nanoclusters for Biomedical and Biosensing Applications: A Mini-Review. *Talanta* **2019**, *200*, 432.
(15) Díaz, S. A.; Hastman, D. A.; Medintz, I. L.; Oh, E. Understanding Energy Transfer with Luminescent Gold Nanoclusters: A Promising New Transduction Modality for Biorelated Applications. *J. Mater. Chem. B* **2017**, *5* (39), 7907.
(16) Zhang, K. Y.; Yu, Q.; Wei, H.; Liu, S.; Zhao, Q.; Huang, W. Long-Lived Emissive Probes for Time-Resolved Photoluminescence Bioimaging and Biosensing. *Chem. Rev.* **2018**, *118* (4), 1770.
(17) Shang, L.; Dong, S.; Nienhaus, G. U. Ultra-Small Fluorescent Metal Nanoclusters: Synthesis and Biological Applications. *Nano Today* **2011**, *6* (4), 401.
(18) Liu, A.; Yang, G.; Liu, Y.; Liu, T. Research Progress in Membrane Fusion-Based Hybrid Exosomes for Drug Delivery Systems. *Front. Bioeng. Biotechnol.* **2022**, *10*, 939441.
(19) Sato, Y. T.; Umezaki, K.; Sawada, S.; Mukai, S.; Sasaki, Y.; Harada, N.; Shiku, H.; Akiyoshi, K. Engineering Hybrid Exosomes by Membrane Fusion with Liposomes. *Sci. Rep.* **2016**, *6* (1), 21933.
(20) Cheng, L.; Zhang, X.; Tang, J.; Lv, Q.; Liu, J. Gene-Engineered Exosomes-Thermosensitive Liposomes Hybrid Nanovesicles by the Blockade of CD47 Signal for Combined Photothermal Therapy and Cancer Immunotherapy. *Biomaterials* **2021**, *275*, 120964.
(21) Tian, Y.; Li, S.; Song, J.; Ji, T.; Zhu, M.; Anderson, G. J.; Wei, J.; Nie, G. A Doxorubicin Delivery Platform Using Engineered Natural Membrane Vesicle Exosomes for Targeted Tumor Therapy. *Biomaterials* **2014**, *35* (7), 2383.
(22) Ayed, Z.; Cuvillier, L.; Dobhal, G.; Goreham, R. V. Electroporation of Outer Membrane Vesicles Derived from Pseudomonas Aeruginosa with Gold Nanoparticles. *SN Appl. Sci.* **2019**, *1* (12), 1600.
(23) Panagopoulou, M. S.; Wark, A. W.; Birch, D. J. S.; Gregory, C. D. Phenotypic Analysis of Extracellular Vesicles: A Review on the Applications of Fluorescence. *J. Extracell. Vesicles* **2020**, *9* (1), 1710020.
(24) Kauscher, U.; Penders, J.; Nagelkerke, A.; Holme, M. N.; Nele, V.; Massi, L.; Gopal, S.; Whittaker, T. E.; Stevens, M. M. Gold Nanocluster Extracellular Vesicle Supraparticles: Self-Assembled Nanostructures for Three-Dimensional Uptake Visualization. *Langmuir* **2020**, *36* (14), 3912.
(25) Chiechio, R. M.; Ducarre, S.; Moulin, G.; Dupont, A.; Marets, C.; Even-Hernandez, P.; Artzner, F.; Musumeci, P.; Franzò, G.; Ravel, C.; LoFaro, M. J.; Marchi, V. Luminescent Gold Nanoclusters Interacting with Synthetic and Biological Vesicles. *J. Phys. Chem. Lett.* **2022**, *13* (30), 6935.
(26) Jhan, Y.-Y.; Prasca-Chamorro, D.; Palou Zuniga, G.; Moore, D. M.; Arun Kumar, S.; Gaharwar, A. K.; Bishop, C. J. Engineered Extracellular Vesicles with Synthetic Lipids via Membrane Fusion to Establish Efficient Gene Delivery. *Int. J. Pharm.* **2020**, *573*, 118802.
(27) Piffoux, M.; Silva, A. K. A.; Wilhelm, C.; Gazeau, F.; Tareste, D. Modification of Extracellular Vesicles by Fusion with Liposomes for the Design of Personalized Biogenic Drug Delivery Systems. *ACS Nano* **2018**, *12* (7), 6830.
(28) Singh, A.; Raghav, A.; Shiekh, P. A.; Kumar, A. Transplantation of Engineered Exosomes Derived from Bone Marrow Mesenchymal Stromal Cells Ameliorate Diabetic Peripheral Neuropathy under Electrical Stimulation. *Bioact. Mater.* **2021**, *6* (8), 2231.
(29) Lentz, B. R. PEG as a Tool to Gain Insight into Membrane Fusion. *Eur. Biophys. J.* **2007**, *36* (4−5), 315.
(30) Lentz, B. R.; Lee, J. Poly(Ethylene Glycol) (PEG)-Mediated Fusion between Pure Lipid Bilayers: A Mechanism in Common with Viral Fusion and Secretory Vesicle Release? (Review). *Mol. Membr. Biol.* **1999**, *16* (4), 279.
(31) Lasic, D. D.; Joannic, R.; Keller, B. C.; Frederik, P. M.; Auvray, L. Spontaneous Vesiculation. *Adv. Colloid Interface Sci.* **2001**, *89*−*90*, 337.
(32) Perissinotto, F.; Rondelli, V.; Senigagliesi, B.; Brocca, P.; Almásy, L.; Bottyán, L.; Merkel, D. G.; Amenitsch, H.; Sartori, B.; Pachler, K.; Mayr, M.; Gimona, M.; Rohde, E.; Casalis, L.; Parisse, P. Structural Insights into Fusion Mechanisms of Small Extracellular Vesicles with Model Plasma Membranes. *Nanoscale* **2021**, *13* (10), 5224.
(33) Karmacharya, M.; Kumar, S.; Cho, Y.-K. Tuning the Extracellular Vesicles Membrane through Fusion for Biomedical Applications. *J. Funct. Biomater.* **2023**, *14* (2), 117.
(34) Morandi, M. I.; Busko, P.; Ozer-Partuk, E.; Khan, S.; Zarfati, G.; Elbaz-Alon, Y.; Abou Karam, P.; Napso Shogan, T.; Ginini, L.; Gil, Z.; Regev-Rudzki, N.; Avinoam, O. Extracellular Vesicle Fusion Visualized by Cryo-Electron Microscopy. *PNAS Nexus* **2022**, *1* (4), 156.
(35) Allen, T. M.; Cullis, P. R. Liposomal Drug Delivery Systems: From Concept to Clinical Applications. *Adv. Drug Delivery Rev.* **2013**, *65* (1), 36.
(36) Uzel, A.; Agiotis, L.; Baron, A.; Zhigaltser, I. V.; Meunier, M.; Kafshgari, M. H.; Cullis, P. R. Single Pulse Nanosecond Laser-Stimulated Targeted Delivery of Anti-Cancer Drugs from Hybrid Lipid Nanoparticles Containing 5 nm Gold Nanoparticles. *Small* **2023**, *19* (52), 230559.
(37) Su, J.; Feng, C.; Wu, Y.; Liang, J. A Novel Gold-Nanocluster-Based Fluorescent Sensor for Detection of Sodium 2-Mercaptoethanesulfonate. *RSC Adv.* **2019**, *9* (33), 18949.
(38) Wu, Z.; Jin, R. On the Ligand's Role in the Fluorescence of Gold Nanoclusters. *Nano Lett.* **2010**, *10* (7), 2568.
(39) Hope, M. J.; Bally, M. B.; Webb, G.; Cullis, P. R. Production of Large Unilamellar Vesicles by a Rapid Extrusion Procedure. Characterization of Size Distribution, Trapped Volume and Ability to Maintain a Membrane Potential. *Biochim. Biophys. Acta BBA - Biomembr.* **1985**, *812* (1), 55.
(40) Chiechio, R. M.; Ducarre, S.; Marets, C.; Dupont, A.; Even-Hernandez, P.; Pinson, X.; Dutertre, S.; Artzner, F.; Musumeci, P.; Ravel, C.; Faro, M. J. L.; Marchi, V. Encapsulation of Luminescent Gold Nanoclusters into Synthetic Vesicles. *Nanomaterials* **2022**, *12* (21), 3875.
(41) Skalnikova, H. K.; Bohuslavova, B.; Turnovcova, K.; Juhasova, J.; Juhas, S.; Rodinova, M.; Vodicka, P. Isolation and Characterization of Small Extracellular Vesicles from Porcine Blood Plasma, Cerebrospinal Fluid, and Seminal Plasma. *Proteomes* **2019**, *7* (2), 17.
(42) Thorsteinsson, K.; Olsén, E.; Schmidt, E.; Pace, H.; Bally, M. FRET-Based Assay for the Quantification of Extracellular Vesicles and Other Vesicles of Complex Composition. *Anal. Chem.* **2020**, *92* (23), 15336.
(43) François-Martin, C.; Bacle, A.; Rothman, J. E.; Fuchs, P. F. J.; Pincet, F. Cooperation of Conical and Polyunsaturated Lipids to Regulate Initiation and Processing of Membrane Fusion. *Front. Mol. Biosci.* **2021**, *8*, 763115.
(44) Martin, F. J.; MacDonald, R. C. Lipid Vesicle-Cell Interactions. II. Induction of Cell Fusion. *J. Cell Biol.* **1976**, *70* (3), 506.
(45) Bebelman, M. P.; Bun, P.; van Niel, G.; Huveneers, S.; Pegtel, D. M.; Verweij, F. J. Real-Time Imaging of Multivesicular Body−Plasma Membrane Fusion to Quantify Exosome Release from Single Cells. *Nat. Protoc.* **2020**, *15*, 102.
(46) Zhigaltsev, I. V.; Tam, Y. Y. C.; Kulkarni, J. A.; Cullis, P. R. Synthesis and Characterization of Hybrid Lipid Nanoparticles Containing Gold Nanoparticles and a Weak Base Drug. *Langmuir* **2022**, *38* (25), 7858.
(47) Dubochet, J.; McDowall, A. W. Vitrification of pure water for electron microscopy. *J. Microscopy* **1981**, *124* (3), 3−4.

https://doi.org/10.1021/acsami.4c02445
ACS Appl. Mater. Interfaces 2024, 16, 21643−21652